Kinetochore–microtubule attachment throughout mitosis potentiated by the elongated stalk of the kinetochore kinesin CENP-E

Benjamin Vitre[a,*], Nikita Gudimchuk[b,*,†], Ranier Borda[a], Yumi Kim[a,‡], John E. Heuser[c,d], Don W. Cleveland[a], and Ekaterina L. Grishchuk[b]
[a]Ludwig Institute for Cancer Research and Department of Cellular and Molecular Medicine, University of California, San Diego, La Jolla, CA 92093; [b]Physiology Department, Perelman School of Medicine, University of Pennsylvania, Philadelphia, PA 19104; [c]Department of Cell Biology, Washington University in Saint Louis, St Louis, MO 63110; [d]WPI Institute for Cell and Material Sciences, Kyoto University, Kyoto 606-8501, Japan

ABSTRACT Centromere protein E (CENP-E) is a highly elongated kinesin that transports pole-proximal chromosomes during congression in prometaphase. During metaphase, it facilitates kinetochore–microtubule end-on attachment required to achieve and maintain chromosome alignment. In vitro CENP-E can walk processively along microtubule tracks and follow both growing and shrinking microtubule plus ends. Neither the CENP-E–dependent transport along microtubules nor its tip-tracking activity requires the unusually long coiled-coil stalk of CENP-E. The biological role for the CENP-E stalk has now been identified through creation of "Bonsai" CENP-E with significantly shortened stalk but wild-type motor and tail domains. We demonstrate that Bonsai CENP-E fails to bind microtubules in vitro unless a cargo is contemporaneously bound via its C-terminal tail. In contrast, both full-length and truncated CENP-E that has no stalk and tail exhibit robust motility with and without cargo binding, highlighting the importance of CENP-E stalk for its activity. Correspondingly, kinetochore attachment to microtubule ends is shown to be disrupted in cells whose CENP-E has a shortened stalk, thereby producing chromosome misalignment in metaphase and lagging chromosomes during anaphase. Together these findings establish an unexpected role of CENP-E elongated stalk in ensuring stability of kinetochore–microtubule attachments during chromosome congression and segregation.

INTRODUCTION

Accurate chromosome segregation in mitosis depends on the dynamic interactions between the kinetochore and spindle microtubules. Kinetochores are complex multiprotein structures that localize at the centromeres of duplicated chromosomes during mitosis. The main function of the kinetochores is to connect chromosomes to the mitotic spindle and mediate signaling the state of this attachment to the cell cycle machinery (Cleveland *et al.*, 2003). One kinetochore component, centromere protein E (CENP-E), is a plus end–directed, microtubule-dependent motor from the kinesin-7 family. Similar to other members of the kinesin superfamily, CENP-E is a homodimer, in which two motor domains are linked with two tail domains via a dimerizing coiled coil. The stalk domain of CENP-E is highly elongated, spanning >200 nm (Kim *et al.*, 2008), significantly longer than in most kinesins. This fibrillar kinesin accumulates before mitosis (Brown *et al.*, 1994), but soluble CENP-E molecules in the cytoplasm of a mitotic cell are believed to be folded and inactive, as the tail of CENP-E can bind the motor domains, inhibiting the microtubule-stimulated ATPase activity (Espeut *et al.*, 2008). Previous work also suggested that the initially autoinhibited CENP-E becomes activated during mitosis via phosphorylation, which disrupts

tail-mediated motor inhibition (Espeut *et al.*, 2008). At mitosis onset, CENP-E also becomes recruited to the outer layer of each kinetochore via its kinetochore-binding site located near its C-terminus (Chan *et al.*, 1998). A fully elongated extension of the active, kinetochore-bound CENP-E may help to increase the span of the amino-terminal motor domain from a bound kinetochore cargo, thereby potentiating capture of spindle microtubules during prometaphase (Kim *et al.*, 2008, 2010; Gudimchuk *et al.*, 2013). At the kinetochores of aligned chromosomes in metaphase, however, the CENP-E is not fully extended, and its conformation changes when the kinetochore is under tension (Wan *et al.*, 2009).

Results of the genetic depletion of CENP-E (Putkey *et al.*, 2002; Weaver *et al.*, 2003), its removal from kinetochores (McEwen *et al.*, 2001), and inhibition of its motor activity (Gudimchuk *et al.*, 2013) implicate CENP-E as an important kinetochore component that contributes to high fidelity of chromosome segregation. CENP-E plays an essential role in transporting pole-proximal chromosomes to the spindle equator during prometaphase, a process called chromosome congression (Yen *et al.*, 1991; Schaar *et al.*, 1997; Wood *et al.*, 1997). The initial congression of misaligned chromosomes takes place along already established kinetochore fibers and along the microtubules directed to the spindle equator (Kapoor *et al.*, 2006; Cai *et al.*, 2009). CENP-E–mediated chromosome motility requires that its motor domain is active (Kim *et al.*, 2008, 2010), but whether other molecular features of this kinetochore protein have important physiological significance in not yet known. In addition to its transporting role during congression, CENP-E has been suggested to play a role in facilitating kinetochore–microtubule attachment during metaphase (Gudimchuk *et al.*, 2013). Consistently, depletion of CENP-E results in 50% decrease in the density of kinetochore fibers in human and mouse cells (McEwen *et al.*, 2001; Putkey *et al.*, 2002). Of interest, the stabilization of kinetochore–microtubule attachment also appears to require CENP-E–dependent localization of other proteins to the kinetochore, especially protein phosphatase 1 (PP1; Kim *et al.*, 2010) and the checkpoint protein BubR1 (Guo *et al.*, 2012). CENP-E–dependent localization of these (and potentially other kinetochore proteins) may help to regulate the dynamics of kinetochore–microtubule interactions and/or signal the state of these attachments to the cell cycle machinery. It has also been suggested that CENP-E is required for normal kinetochore–microtubule attachment during anaphase, since a genetic depletion of CENP-E from cells in regenerating mouse liver and embryonic fibroblasts in culture results in an increased frequency of lagging chromosomes (Putkey *et al.*, 2002; Weaver *et al.*, 2003).

Much of the molecular information about the CENP-E kinesin has also been learned from motility assays in vitro. Molecules of purified full-length CENP-E protein show heterogeneous behavior on a microtubule wall: whereas many CENP-E molecules bind microtubules transiently and show diffusive motion, some motors walk unidirectionally and processively (Gudimchuk *et al.*, 2013). The heterogeneity of single CENP-E molecules is consistent with the idea that the CENP-E tail can inhibit its own motor domain and that these interactions are transient. Indeed, the reported dissociation constant of 3 μM for purified tail and head domains suggests weak binding (Espeut *et al.*, 2008). Of importance, truncated versions of CENP-E, which completely lack the elongated stalk and C-terminal tail, can walk well along a microtubule and transport microbeads, thereby mimicking the activities of the active molecules of full-length CENP-E and indicating that the stalk and tail have little effect during CENP-E's walking (Kim *et al.*, 2008; Yardimci *et al.*, 2008; Gudimchuk *et al.*, 2013). However, whereas full-length CENP-E can associate processively with the ends of dynamic microtubules in

vitro, the truncated motor falls off microtubule ends and fails to track (Gudimchuk *et al.*, 2013). Of interest, when purified tail and motor domains are joined together using Quantum Dots, this produces conjugates that walk well along a microtubule wall and are able to recapitulate the processive association with the plus end of dynamic microtubules characteristic of full-length CENP-E (Gudimchuk *et al.*, 2013). These experiments suggested that neither the tip-tracking activity nor the CENP-E–dependent transport along a microtubule wall in vitro requires the elongated stalk of CENP-E, raising a question about its contribution to CENP-E functions. Through creation of "Bonsai" versions of CENP-E in which its stalk is significantly shortened but wild-type motor and tail domains are retained, we now identify the biological role for the CENP-E stalk.

RESULTS
CENP-E coiled-coil stalk regulates motor function in vitro
Previous structural work visualizing purified CENP-E dimers with electron microscopy reported that soluble CENP-E can adopt many different conformations (Kim *et al.*, 2008), consistent with a highly flexible coiled-coil region. Direct examination of full-length *Xenopus* CENP-E by electron microscopy using quick-freeze deep-etch and platinum replication (Heuser, 1989) identified a small proportion of CENP-E molecules in a folded conformation in which the extended stalk domain was looped and the head and tail appeared to be bound (Figure 1A, bottom). The low incidence of folded molecules may reflect the transient nature of this configuration, since binding between purified head and tail domains is weak (Espeut *et al.*, 2008).

To determine whether the flexible elongated stalk of CENP-E is essential for its function, we characterized the activity of a "Bonsai" CENP-E in which 1475 amino acids (aa) of the ~1700 aa CENP-E coiled-coil domain were removed, thus shortening the stalk by 85% (Figure 1B). This shorter stalk contains the minimal segment that is sufficient for CENP-E dimerization and is predicted to form short discontinuous coiled coil (Supplemental Figure S1A). Bonsai CENP-E was expressed in insect cells, leading to production of the expected 197-kDa product (Supplemental Figure S1B). First, we tested whether Bonsai CENP-E could power the movement of microtubules in a traditional gliding assay in vitro. Bonsai CENP-E was attached to a coverslip using an antibody to its C-terminal green fluorescent protein (GFP) tag, and motions of stabilized fluorescent microtubules were recorded in the presence of ATP (Supplemental Figure S1C). This mutant retained robust motor activity, although the gliding rate and the percentage of moving microtubules were reduced compared with truncated CENP-E that lacked the entire stalk and tail (Figure 1, C and D). We next used the same conjugation strategy to attach Bonsai protein to microbeads. Laser tweezers were used to bring the beads in contact with coverslip-attached microtubules, and their mobility was assessed via differential interference contrast (DIC) microscopy (Figure 1E and Supplemental Figure S1D). This approach confirmed that Bonsai CENP-E transported cargo along microtubule tracks with a reduced velocity relative to either truncated or full-length CENP-E, producing microbead transport velocities of 5.9 ± 0.5, 17.1 ± 1.6, and 19.2 ± 2.1 μm/min, respectively (Figure 1E). We conclude that cargo-conjugated Bonsai CENP-E could support microtubule motility, but with a reduced velocity.

Strikingly different results were seen when we used total internal reflection fluorescence (TIRF) microscopy to visualize how cargo-free molecules of Bonsai CENP-E interacted with microtubules (Supplemental Figure S1E). Previous work with truncated CENP-E established that soluble molecules of this dimeric motor readily bind and walk on microtubules, whereas the full-length
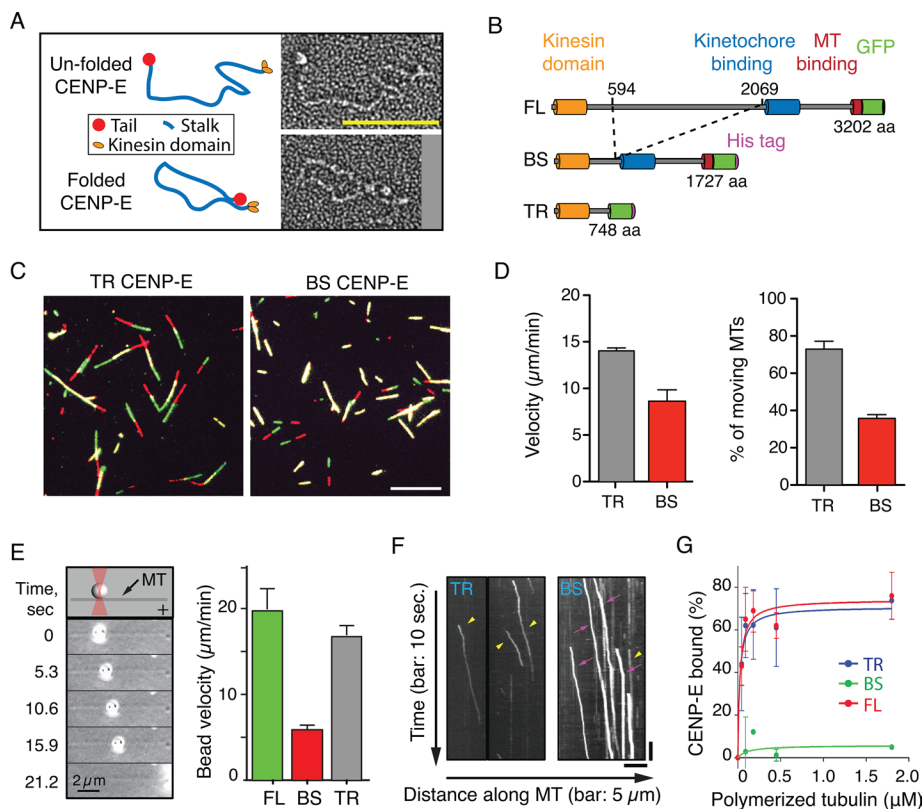
FIGURE 1: In vitro characterization of Bonsai CENP-E functions. (A) Schematics and electron micrographs of individual full-length CENP-E molecules. Our analysis of electron micrographs shows that 3.6% of CENP-E molecules (total $N = 84$) appear folded. Scale bar, 100 nm. (B) Schematic of full-length (FL), Bonsai (BS), and truncated (TR) CENP-E constructs. C-terminal tail of CENP-E has both a microtubule (MT)-binding site and a motor-binding domain (not shown), which can bind to the motor domain, inhibiting its activity. (C) Representative images of microtubule fields for different CENP-E coverslips. Colored overlays compare microtubules images at different times: red, initial positions; green, 2 s later. Scale bar, 5 μm. (D) Velocity and percentage of moving microtubules for truncated and Bonsai CENP-E. Bars, median ± SEM. At least five independent microscopy chambers were analyzed with truncated and two chambers with Bonsai CENP-E; 10–45 microtubules were analyzed for each chamber. (E) Schematic and montage of stills from a time-lapse of Bonsai CENP-E–coated bead visualized with DIC. Numbers is time in seconds from the start of the bead's motion. Diagram shows velocity of beads coated with full-length, Bonsai, and truncated CENP-E. Bars, mean ± SEM; based on 26 beads for full-length, 20 for Bonsai, and 57 for truncated CENP-E proteins. Data for truncated and full-length CENP-E are from Gudimchuk *et al.* (2013). (F) Representative kymographs for truncated and Bonsai CENP-E molecules moving on Taxol-stabilized microtubules recorded under identical experimental conditions. Yellow arrowheads point to less bright complexes, which, based on quantitative analysis of fluorescence intensity, represent one or two CENP-E dimers. In Bonsai CENP-E chambers, only larger molecular clusters show directed motility (pink arrows), presumably because occasionally such protein clusters contain uninhibited CENP-E motor heads. (G) Microtubule affinity of truncated, Bonsai, and full-length CENP-E measured in a fluorescence-based pelleting assay with AMPPNP. Mean ± SEM, based on two or more independent experiments. K_d values are reported with 95% confidence.

molecules either diffuse or walk processively (Kim *et al.*, 2008; Gudimchuk *et al.*, 2013). In contrast to both of these constructs, we observed no binding between Bonsai CENP-E molecules and microtubules; consequently, there was no detectable motion of Bonsai CENP-E along a microtubule wall or the tip tracking at the microtubule end that is characteristic of full-length CENP-E. Occasionally we observed processive motion of fluorescent complexes, which, based on their brightness, contained multiple molecules of Bonsai CENP-E, confirming that this protein was capable of moving on microtubules under these assay conditions (Figure 1F, pink arrows, and Supplemental Figure S1F). The lack of

single-molecule walking on microtubules appeared to result from a reduced association rate between Bonsai and microtubules, as numerous motor molecules were present in the solution and could be seen attached nonspecifically to the coverslip (Supplemental Figure S1G). The initial brightness of these dots and the number of photobleaching steps were highly similar to those seen for dimeric kinesin 1 motor but not for the monomers of Ndc80-GFP protein (Supplemental Figure S1, H–J). Together these results demonstrate that Bonsai CENP-E dimerizes but fails to bind to microtubules.

Of importance, the inhibition of microtubule binding by soluble, cargo-free Bonsai CENP-E dimers was stronger than that seen with full-length CENP-E, which differs from Bonsai only in the length of the flexible stalk. When we carried out a microtubule-pelleting assay in the presence of AMPPNP, a nonhydrolyzable analogue of ATP known to induce rigor binding of motor heads (Liao *et al.*, 1994), both full-length and truncated CENP-E proteins bound strongly to microtubules ($K_d = 24 ± 10$ and $23 ± 7$ nM, respectively). However, Bonsai CENP-E showed almost no binding (Figure 1G), confirming that in the absence of a cargo, this mutant protein has a highly reduced affinity to microtubules. Together these assays revealed that elongated flexible stalk of CENP-E plays an important role in regulating its motor activity in vitro.

Elongated stalk is essential for efficient chromosome congression via an CENP-E–dependent mechanism

Previous work using *Xenopus* egg extracts and cells revealed that motor activity of CENP-E is essential for chromosome congression (Kim *et al.*, 2008, 2010). Indeed, a CENP-E "rigor" mutant, which stably binds to the microtubules and cannot walk, is not capable of mediating congression (Kim *et al.*, 2008). In addition, it was proposed that CENP-E could promote congression by facilitating capture of already established bundles of kinetochore microtubules due to its highly elongated and flexible coiled-coil stalk (Kim *et al.*, 2008). To examine the in vivo function of the CENP-E stalk during congression in human cells, we created several cell lines expressing different versions of Bonsai CENP-E (Figure 2A and Supplemental Figure S2A).

A gene encoding each of these mutants (which differed in the length of the CENP-E stalk), as well as full-length CENP-E (Kim *et al.*, 2010), was integrated at a specific genomic locus in human DLD-1 cells using the FRT/Flp-mediated recombination Flip-In system. Next endogenous CENP-E, which undergoes cell cycle–dependent accumulation and loss that mimics that of cyclin B (Brown *et al.*, 1994), was depleted using small interfering RNA (siRNA) directed
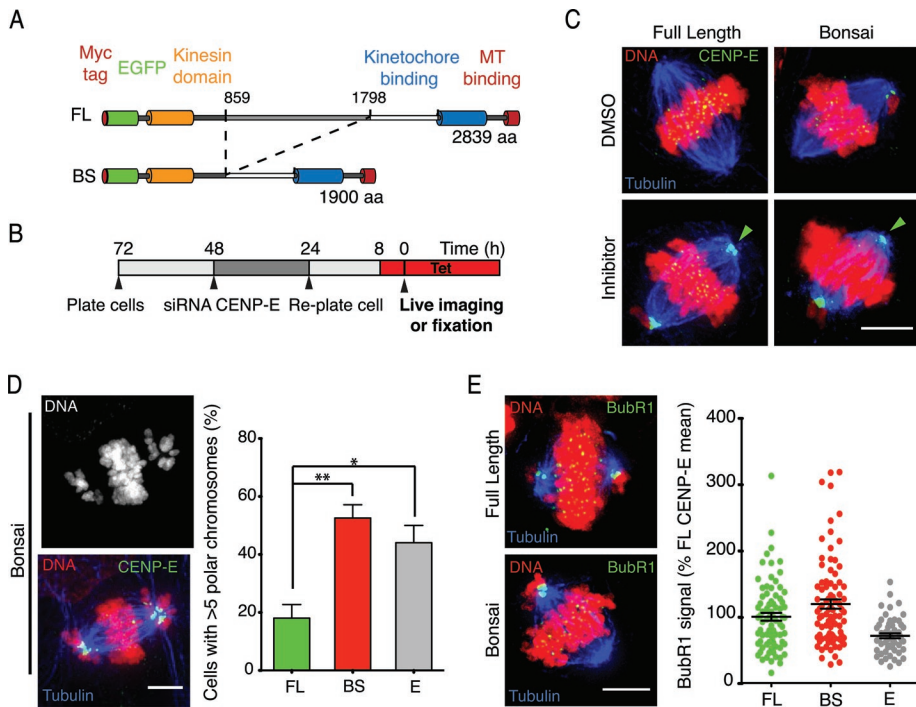
FIGURE 2: Analysis of Bonsai CENP-E functions in prometaphase. (A) Schematic of the full-length and Bonsai Myc-Lap-GFP–tagged CENP-E proteins used in DLD-1 cells. (B) Schematic of experimental timeline to prepare cells for endogenous CENP-E depletion, Bonsai or full-length CENP-E rescue and imaging. (C) Representative images of two cells depleted of endogenous CENP-E and expressing full-length or Bonsai CENP-E in the presence of DMSO or CENP-E inhibitor GSK 923295. Green arrowheads point to CENP-E accumulated at the spindle poles. Scale bar, 5 µm. (D) Representative image of a cell with depleted endogenous CENP-E and expressing the Bonsai CENP-E; note the presence of polar chromosomes. Graph shows the average percentage of cells with more than five polar chromosomes. Here and elsewhere, "E" is a control (empty) condition when cells were not rescued. Error bars, SEM; **$p < 0.01$; *$p < 0.05$; p value of unpaired t test realized on the mean of two (empty) or three (full-length and Bonsai) independent experiments; $N = 69$ cells for empty, 158 for Bonsai, and 92 for full-length CENP-E. Scale bar, 5 µm. (E) Representative image of BubR1 immunostaining of DLD-1 cells, which were depleted of endogenous CENP-E and induced to express the Bonsai or full-length CENP-E protein. Graph representing BubR1 signal intensity at the kinetochore of unaligned chromosomes in different cells. $N = 78$ unaligned kinetochores were measured for full-length CENP-E (from 10 cells), 87 for Bonsai (14 cells), and 53 for empty (6 cells). Scale bar, 5 µm.

against the 3' untranslated region of the endogenous CENP-E mRNA (Kim et al., 2010), and the cells were "rescued" by inducing either full-length or Bonsai myc-tagged-GFP CENP-E proteins by addition of doxycycline for 8 h (Figure 2B). Induction by addition of doxycycline led to comparable accumulation level of each variant (Supplemental Figure S2B). Both long and medium Bonsai CENP-E displayed normal kinetochore localization, and each was enriched at kinetochores of unaligned chromosomes. Short Bonsai CENP-E showed highly reduced kinetochore signal (Supplemental Figure S2C). To examine the growth of these Bonsai CENP-E cell lines, we performed a clonogenic assay in cells incubated in doxycycline for >15 d. Expression of medium Bonsai CENP-E resulted in fewer colonies, consistent with a stronger perturbation of mitotic cell division (Supplemental Figure S2D), and so this construct was used for more-detailed characterization.

Because our in vitro data indicated that shortening its stalk disrupted CENP-E binding to microtubules, we first tested whether the kinetochore-bound shortened CENP-E was capable of interacting with microtubules directly. Cells were treated with GSK923295, a small-molecule inhibitor of CENP-E, which locks its kinesin motor in

a "rigor" state, strongly bound to microtubules (Wood et al., 2010). In cells rescued with full-length CENP-E, this treatment caused a loss of kinetochore-bound CENP-E and its accumulation at the poles of the mitotic spindle after passive translocation via poleward microtubule flux (Gudimchuk et al., 2013). After treatment with the CENP-E inhibitor, Bonsai CENP-E also accumulated at the spindle poles, revealing that the kinetochore-bound Bonsai was still able to bind to microtubules and adopt a rigor-like state (Figure 2C).

To evaluate whether Bonsai CENP-E could support normal congression of polar chromosomes, we quantified the proportion of cells with an elevated number of polar chromosomes (more than five). A threefold increase in the number of cells with polar chromosomes was seen with Bonsai CENP-E relative to rescue with full-length CENP-E (52 ± 5 vs. 18 ± 5%; Figure 2D), indicating significant loss of CENP-E-dependent congression. The elevated number of polar chromosomes in cells rescued with Bonsai CENP-E triggered a strong activation of the mitotic checkpoint, as the average mitotic duration increased twofold compared with cells depleted of CENP-E (300 ± 29 vs. 163 ± 31 min; Supplemental Figure S2E). This delay suggested that Bonsai CENP-E could still preserve functionality of the mitotic checkpoint (Abrieu et al., 2000; Mao et al., 2003).

To test this further, we measured the recruitment of BubR1 at the kinetochores of polar chromosomes in cells rescued with Bonsai CENP-E, since wild-type CENP-E has been shown to contribute to BubR1 targeting (Weaver et al., 2003). Quantitative immunofluorescence measurements revealed comparable accumulation of BubR1 at the kinetochores of unaligned chromosomes in full-length and Bonsai-rescued cells, whereas cells depleted of CENP-E displayed 50% reduction in BubR1 signal at kinetochores of polar chromosomes (Figure 2E). Thus, these assays revealed that in a cellular context, Bonsai CENP-E retained ability to 1) localize to kinetochores (thus attaching to its cargo), 2) bind to microtubules and produce a rigor phenotype in the presence of its specific inhibitor, including passive accumulation at poles, and 3) support normal mitotic checkpoint activity. Nevertheless, Bonsai CENP-E missing the extended coiled-coil was unable to support efficient congression of polar chromosomes.

CENP-E motor function is required for stabilization of kinetochore–microtubule attachment in metaphase

In addition to its role in chromosome congression, CENP-E potentiates stabilization of kinetochore–microtubule attachment. The initial evidence for this was that depletion of CENP-E resulted in 50% reduction of kinetochore microtubule fibers of fully congressed, metaphase chromosomes (McEwen et al., 2001; Putkey et al., 2002). Further, genomic deletion of CENP-E led to
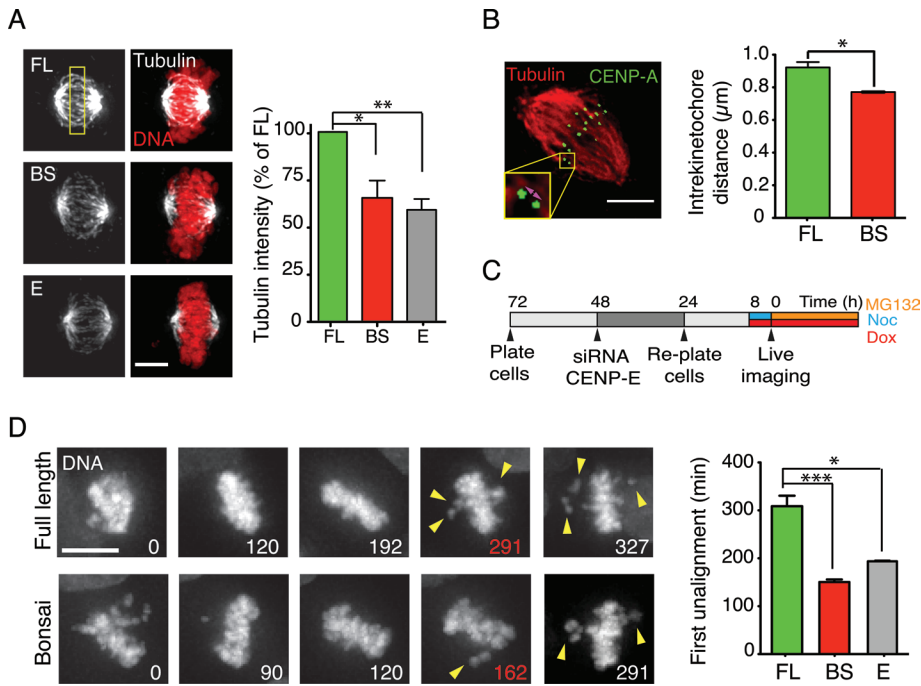
FIGURE 3: Reduced stability of kinetochore–microtubule attachment in metaphase in cells expressing Bonsai CENP-E. (A) Representative images of mitotic cells arrested at metaphase with proteasome inhibitor MG132 and subjected to cold for 20 min. Cells were depleted of endogenous CENP-E and rescued with the Bonsai or full-length CENP-E or not rescued. Yellow frame indicates area where tubulin intensity was measured. Scale bar, 4 µm. Right, mean intensity of tubulin signal for cells submitted to cold; *$p < 0.05$, **$p < 0.01$; p value of unpaired t test realized on the mean of three independent experiments. $N = 78$ cells were analyzed for full-length, 107 for Bonsai, and 70 for empty condition. (B) Representative image used for interkinetochore distance measurement. Purple double-arrowhead indicates the interkinetochore distance. Scale bar, 5 µm. Diagram represents the mean interkinetochore distance in cells depleted of endogenous CENP-E expressing full-length and Bonsai CENP-E. *$p < 0.05$, p value of unpaired t test realized on the mean of two independent experiments. We analyzed 248 kinetochores from 9 cells for full length and 272 from 10 cells for Bonsai. (C) Schematic illustrating timing of cell plating and drug treatment used for experiments in D. Cells were arrested at metaphase with MG132 and imaged live. Noc, nocodazole; Dox, doxycycline. (D) Still images from Supplemental Videos S1 (Full Length) and S2 (Bonsai) showing loss of chromosome alignment (yellow arrowheads) after the chromosomes congressed to the spindle equator. Numbers are time in minutes; scale bar, 10 µm. Right, average time from nocodazole release to first chromosome unalignment event in cells treated as in C. Bars represent the mean time to the first unalignment of chromosome. $N = 78$ and 58 cells for full-length and Bonsai CENP-E, respectively, based on three independent experiments; $N = 33$ cells for empty condition based on two independent experiments; ***$p < 0.001$; p value of an unpaired t test realized on the mean of three independent experiments. Error bars, SEM.

lagging chromosomes in mouse embryonic fibroblast and cells of regenerating liver (Putkey *et al.*, 2002; Weaver *et al.*, 2003). Finally, in a recent effort, two different approaches (depletion of CENP-E by RNA interference and drug-induced inhibition of CENP-E to inactivate motor activity and displace it from kinetochores) were used to demonstrate that the CENP-E motor facilitates kinetochore–microtubule attachment in metaphase and during induced microtubule depolymerization (Gudimchuk *et al.*, 2013). Reduced kinetochore–microtubule stability after low temperature–induced microtubule depolymerization has also been found for other kinetochore microtubule-binding proteins, including the NDC80 complex (DeLuca *et al.*, 2006), suggesting that CENP-E functions in protecting kinetochore microtubule ends from cold-induced disassembly and detachment.

We tested whether kinetochore-bound Bonsai CENP-E retained this ability. Cells rescued with Bonsai or full-length CENP-E were arrested in metaphase using MG132 (to impose mitotic arrest, whether or not the mitotic checkpoint signal was active) and subjected to cold treatment for 20 min. Compared to the full-length CENP-E control, cells rescued with Bonsai CENP-E displayed a 30% reduction of cold-stable microtubules, a level comparable to cells depleted of CENP-E (Figure 3A). This result indicated that Bonsai CENP-E was deficient in protecting microtubule ends from cold-induced disassembly. Consistent with the reduced density of cold-stable kinetochore–microtubules, measurement of interkinetochore distances in unperturbed metaphase cells revealed that they were significantly shorter in cells rescued with the Bonsai motor (Figure 3B).

Next we assessed whether the presence of Bonsai CENP-E affected the maintenance of chromosome biorientation at metaphase. Cells were arrested with MG132, as before, and chromosome alignment was monitored by live-cell imaging (Figure 3, C and D, and Supplemental Videos S1 and S2). Cells rescued with full-length CENP-E maintained proper chromosome biorientation for ~300 min before losing metaphase chromosome alignment, with multiple DNA masses separating simultaneously, a phenotype known as chromosome scattering due to loss of cohesion (Daum *et al.*, 2011; Stevens *et al.*, 2011). In cells rescued with Bonsai CENP-E, however, loss of chromosome alignment occurred much more quickly, with timing comparable to that in cells with no CENP-E rescue (150 and 190 min, respectively). The premature loss of chromosome alignment in Bonsai CENP-E cells affected fewer chromosomes and increased slowly over time, indicative of defective kinetochore microtubule attachment rather than a cohesion defect. These findings indicate that Bonsai CENP-E cannot properly stabilize chromosome alignment, supporting the idea that presence of a wild-type stalk is important for CENP-E–dependent stability of kinetochore–microtubule attachments in metaphase.

CENP-E motor function is required for stabilization of kinetochore–microtubule attachment in anaphase

To assess whether regulation of CENP-E motor function by its stalk influenced the ability of kinetochores to track and maintain attachment with depolymerizing microtubules ends, we arrested cells rescued with full-length or Bonsai CENP-E in mitosis in the presence of an inhibitor (S-trityl-L-cysteine [STLC]) of the kinesin motor Eg5 (Figure 4A). This treatment induces monopolar spindles with chromosome rosettes and favors establishment of attachment of their kinetochores to the ends of microtubules (Figure 4, B and C, no depolymerization). The cells were then cooled for 20 min to induce depolymerization of nonstabilized microtubules. In monopolar cells, however, this treatment also induced shortening of kinetochore
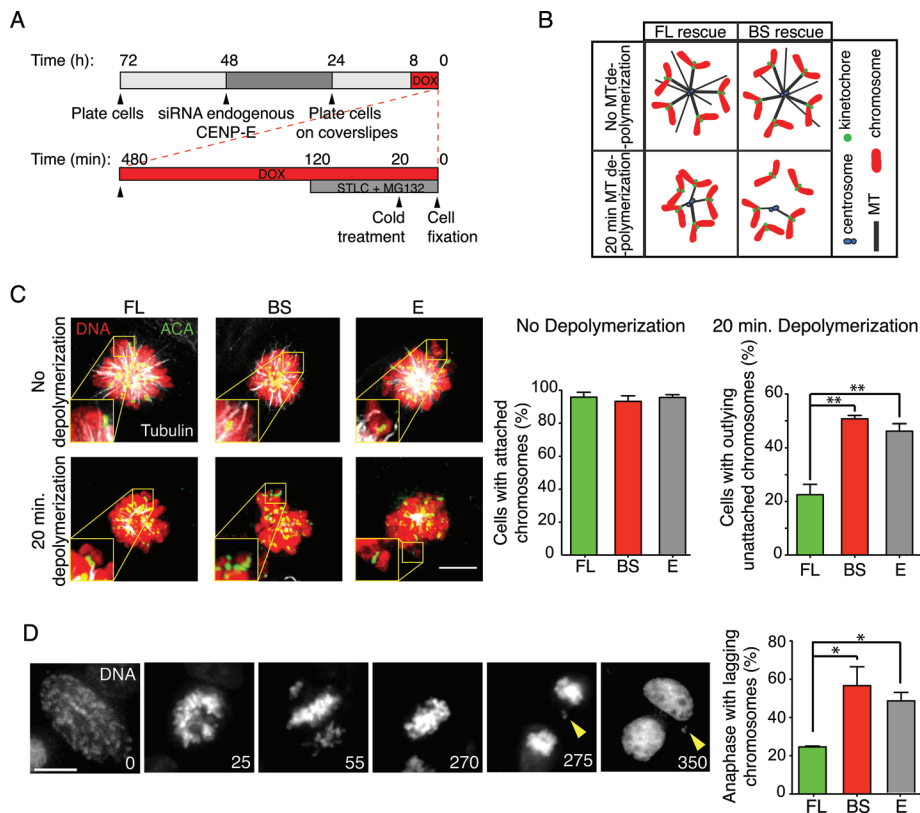
FIGURE 4: Reduced stability of kinetochore–microtubule attachment in anaphase in cells expressing Bonsai CENP-E. (A) Schematic of the cell plating, RNA interference treatment, and drug treatment for the microtubule destabilization assay. (B) Schematic of the microtubule destabilization assay to test kinetochore attachments. The schematic also presents the outcome of the experiment. (C) Representative image of cells rescued with full-length or Bonsai CENP-E, then tested for stability of kinetochore attachments to depolymerizing microtubule ends as in B. Scale bar, 5 µm. Right, percentage of cells with attached chromosomes without microtubule depolymerization and percentage of cells with unattached outlying chromosomes after 20 min of microtubule depolymerization. Error bars, SEM. **$p < 0.01$, p value of a unpaired Student's t test realized on the mean of four (Full Length and Empty) or three (Bonsai) independent experiments. For the 20 min depolymerization condition, $N = 98$ cells were analyzed for full-length, 77 for Bonsai, and 97 for Empty conditions. Anti–centromere antibody (ACA) was used to identify centromeres/kinetochores. (D) Representative images from the time-lapse sequence of a cell with a lagging chromosome (yellow arrowhead). Scale bar, 10 µm. Right, quantification of anaphase cells with lagging chromosomes. Cells were depleted of endogenous CENP-E and rescued with full-length or Bonsai CENP-E or not rescued (Empty); *$p < 0.05$, p value of a unpaired Student's t test realized on the mean of three independent experiments. $N = 130$ cells were analyzed for full-length, 58 for Bonsai, and 97 for Empty conditions.

microtubules and resulted in tightening of chromosome rosettes due to poleward chromosome motion (Gudimchuk et al., 2013). Cells rescued with Bonsai CENP-E had significantly more unattached chromosomes at the periphery of the chromosome rosettes than cells with full-length CENP-E (outlying unattached chromosomes; Figure 4, B and C, 20 min depolymerization).

The necessity of fully functional CENP-E at kinetochores, with its ability to potentiate stable end-on kinetochore–microtubule attachments, was then examined during an unperturbed mitosis. Chromosome motions during anaphase were monitored by live-cell imaging in cells rescued with full-length or Bonsai CENP-E. An increased proportion of cells with lagging chromosomes was observed in cells with Bonsai CENP-E compared with full-length CENP-E (57 ± 10 vs. $25 \pm 1\%$; Figure 4D). Together, these results suggest that a fully elongated CENP-E stalk is required to maintain

stable contact between the kinetochore and depolymerizing microtubule ends. Because of the reduced motor capacity observed for Bonsai CENP-E in vitro (Figure 1 and Supplemental Figure S1), we propose that the unstable kinetochore–microtubule interaction observed in cells expressing Bonsai CENP-E lacking a fully elongated stalk could also be explained by its reduced motor capacity in vivo.

DISCUSSION

The elongated flexible stalk of CENP-E regulates its microtubule binding and motility

Analogous to what was proposed for kinesin 1 (Verhey and Hammond, 2009), previous work with CENP-E established that binding between the head and tail domains of soluble CENP-E can inhibit its ATPase activity, with inhibition relieved by phosphorylation of the CENP-E tail by mitotic kinases (Espeut et al., 2008). Our work identifies two additional mechanisms that are likely to contribute to the regulation of CENP-E activity in cells during mitotic progression. First, similar to kinesins 1 and 3 (Blasius et al., 2007; Yamada et al., 2007), the activity of CENP-E, full length (Gudimchuk et al., 2013) and Bonsai (this work), increases in vitro when its tail is bound to a cargo. Thus, CENP-E binding to kinetochores is likely to be required for activating this motor, ensuring that only the kinetochore-bound CENP-E molecules actively interact with and move along microtubules. Second, our study implicated the CENP-E stalk in regulating microtubule binding and motility of CENP-E. Indeed, in contrast to both full-length and truncated CENP-E motors, soluble molecules of Bonsai CENP-E are strongly defective in microtubule binding in vitro. This result implies that in the context of a full-length molecule the stalk acts as a positive regulator of interactions between microtubules and both of the CENP-E's microtubule-binding sites, one in its motor and a second in its tail.

The absence of motility of soluble molecules of Bonsai CENP-E in vitro, despite supporting robust motility in the gliding and bead assays, could in principle result from reduced dimerization of the shortened stalk of CENP-E. We do not favor this possibility because even our shortest Bonsai constructs have a fairly long region that is predicted to form a coiled coil, including a fragment that has been shown to be sufficient for dimerization (Kim et al., 2008). In addition, Bonsai CENP-E failed to bind microtubules in the presence of AMP-PNP, whereas this nucleotide induces strong binding of both dimeric and monomeric kinesin (Huang and Hackney, 1994; Huang et al., 1994). Finally, our fluorescence analysis of Bonsai CENP-E molecules demonstrates directly that soluble Bonsai can form dimers, so the absence of either directed or diffusive motions of Bonsai CENP-E on microtubules appears to result from strong intramolecular inhibition.
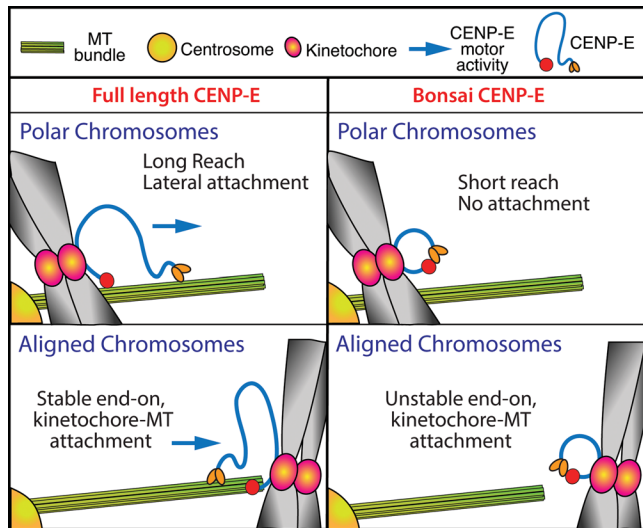
FIGURE 5: Model for the role of CENP-E stalk during mitotic progression. This schematic emphasizes a proposed role of elongated CENP-E stalk during prometaphase in facilitating a microtubule capture by the kinetochores of polar chromosomes, thereby helping to initiate chromosome congression. Our experiments in vitro demonstrate that CENP-E coiled-coil stalk is a positive regulator of CENP-E interactions with microtubules, which may explain why Bonsai CENP-E is not fully active in vivo and induces marked reduction in the stability of kinetochore–microtubule attachments during both metaphase and anaphase. See the text for an extended discussion of other possible molecular mechanisms for the role of CENP-E stalk.

The molecular mechanism of the stalk-mediated regulation of CENP-E microtubule-dependent activity is not yet known, but this effect is likely to result from the unusual structural and biomechanical properties of this coiled-coil domain. The motor domains of all kinesins share a significant similarity, but there are some interesting differences in the properties of their dimerizing stalks (Verhey and Hammond, 2009). The stalk of kinesin 1, for example, is approximately three times shorter than that of CENP-E; perhaps more important, the central portion of kinesin 1's stalk is represented by a rigid coiled coil with a centrally located hinge (Coy et al., 1999; Jeppesen and Hoerber, 2012). This hinge is highly flexible and allows the stalk to fold completely, so that the tail domains bind back on to the heads, promoting autoinhibition, which in turn can be down-regulated by kinesin's light chain (Wong and Rice, 2010; Kaan et al., 2011). In contrast, the elongated stalk of CENP-E is composed of a discontinuous coiled coil, which appears to be highly flexible (Kim et al., 2008). The stalk may directly impinge on the interactions between head and tail of CENP-E, causing repression of autoinhibition akin to the action of the light chain of kinesin 1. In wild-type CENP-E the stalk appears to partially suppress the intramolecular binding between the head and tail, thereby allowing each of these domains to engage in binding to microtubules. We propose that shortening of the stalk reinforces the head-to-tail interaction in CENP-E and strengthens autoinhibition of the motor's activity (Figure 5).

Our hypothesis of a negative role of the CENP-E stalk in autoinhibition explains why the binding of soluble Bonsai molecules to microtubules is inhibited more significantly than seen for the full-length CENP-E molecules and why cargo-free Bonsai CENP-E supports neither directed motility (motor head mediated) nor diffusive motion (tail mediated). The role of CENP-E stalk in mediating the intramolecular interactions is also supported by the lack of microtubule-binding activity of Bonsai CENP-E even in the presence of

AMPPNP, implying that the ATP-binding site of soluble Bonsai CENP-E is blocked. Full-length CENP-E, however, is induced to bind strongly to microtubules by this nonhydrolyzable ATP analogue (Figure 1G). Of interest, when the C-terminal GFP at the tail of CENP-E is conjugated via antibodies to the surface of either a bead or a coverslip, Bonsai CENP-E can bind and walk on microtubules, but still with reduced capabilities. This result suggests that effect of the stalk configuration is less pronounced with cargo-bound versus free CENP-E tail. Finally, the reduced speed of motility with Bonsai CENP-E in multiple motor assays (such as microtubule gliding) can also be attributed to a fraction of inhibited molecules present under these experimental conditions.

Mechanisms of CENP-E–mediated stabilization of kinetochore–microtubule attachments

Our experiments in cells demonstrate that shortening the CENP-E stalk causes a severe reduction in its cellular functions. Although Bonsai CENP-E is recruited robustly to the mitotic kinetochores and exhibits normal enrichment at the kinetochores of pole-proximal chromosomes, in virtually all functional assays this shortened motor produces phenotypes that are similar to or even stronger than those seen with full CENP-E depletion. Indeed, lack of the congression of pole-proximal chromosomes during prometaphase (Figure 2D), reduced stability of kinetochore–microtubule attachments in metaphase (Figure 3), and presence of lagging chromosomes in anaphase (Figure 4) strongly suggest that CENP-E stalk is required for normal CENP-E functioning. These results emphasize the important roles that CENP-E kinesin plays during different mitotic stages, but they also raise a question about why these effects appear to be more severe than in the motility assays in vitro. Indeed, whereas purified Bonsai motor maintains a fairly robust velocity of microtubule gliding and microbead motions in vitro (Figure 1, C–E), it fails to support congression of the poleward chromosomes in cells. Of importance, using the CENP-E inhibitor GSK 923295, we confirmed that the kinetochore-bound Bonsai CENP-E was able to engage in microtubule binding similar to that of full-length CENP-E, demonstrating that the lack of normal mitotic functions of Bonsai CENP-E was not due to a complete inhibition of its microtubule-binding activity.

The rate of bead motions by Bonsai CENP-E in vitro is slower than that of full-length CENP-E, but it seems unlikely that this alone could explain the strong perturbation of kinetochore–microtubule interactions in cellular assays. Bonsai CENP-E motor may have some other important biomechanical defect, which has not yet been revealed by our motility assays in vitro, including reduced processivity of Bonsai CENP-E under a load. We also note that the in vitro and in vivo situations differ in the location of GFP tags and the exact mode of cargo binding: in vitro it takes place at a C-terminal tag, whereas Bonsai CENP-E is bound to its chromosomal cargo via the kinetochore-binding site, which is located upstream from the microtubule-binding site (Figure 1B). It has also been suggested that CENP-E function in vivo requires the long reach that is provided by the extended CENP-E coiled coil (Kim et al., 2008). This length may be important for the capture of already established kinetochore microtubule bundles and efficient congression of polar chromosomes in prometaphase, because a longer stalk could expand the range of microtubule search and capture at each kinetochore early in mitosis (Figure 5, polar chromosomes). The elongated shape of CENP-E may also be important later in mitosis when CENP-E facilitates maintenance and/or capture of new microtubules at the kinetochores of already congressed chromosomes (Figure 5, aligned chromosomes). Thus, a relatively active but short CENP-E motor may not be able to carry out its cellular functions well.

A lack of normal motor activity is expected to reduce the ability of CENP-E to track with dynamic microtubule ends and stabilize end-on attachments, since microtubule tip tracking by CENP-E relies in part on its active motor (Gudimchuk et al., 2013). Indeed, we observed unstable chromosome alignment in metaphase and segregation defects in anaphase in cells rescued with Bonsai CENP-E. We note, however, that destabilization of the end-on kinetochore–microtubule attachments could also result from impaired interaction between CENP-E and some other kinetochore protein(s), including PP1 and Ndc80 (Kim et al., 2010). If in Bonsai CENP-E cells the BubR1 inhibition of Aurora B is reduced (Guo et al., 2012), this could also lead to indirect destabilization of kinetochore microtubule attachment via enhanced Ndc80 phosphorylation. Finally, kinetochore–microtubule attachment defects in cells with Bonsai CENP-E can result from a lack of normal functioning of CENP-E–associated proteins that are required for the stability of kinetochore–microtubule attachments, such as CLASPs (Maffini et al., 2009; Maia et al., 2012) and SKAP (Huang et al., 2012). These possibilities are not mutually exclusive; future work is needed to dissect the mechanism(s) of action of the unusually elongated stalk of CENP-E.

Concluding remarks

We provide several lines of evidence that cells expressing CENP-E with a shortened coiled-coil stalk have aberrant kinetochore–microtubule attachments, which lead to defects in chromosome congression during prometaphase, unstable chromosome biorientation in metaphase, and the presence of lagging chromosomes in anaphase. These results highlight the importance of elongated CENP-E kinesin in facilitating kinetochore–microtubule attachments during all mitotic stages, not just in prometaphase. Our work provides new mechanistic insights into the functions of a protein, perturbations of which had been linked to chromosome segregation errors, aneuploidy, and the development of tumors (Putkey et al., 2002; Weaver et al., 2007; Silk et al., 2013). Our findings could help in understanding the in vivo effects of the drugs that have been developed to target these functions (Ding et al., 2010; Wood et al., 2010).

MATERIALS AND METHODS
Cell culture and cell imaging

Cells were maintained at 37°C with 5% CO_2 in DMEM containing 10% tetracycline-free fetal bovine serum (Clontech, Moutain View, CA), 100 U/ml penicillin, 100 U/ml streptomycin, and 2 mM L-glutamine. The CENP-E rescue experiment was performed using the human CENP-E constructs cloned in a pcDNA5/FRT/TO vector (Invitrogen, Carlsbad, CA), generated as described in Kim et al., 2010. Doxycycline was used at 1 mg/ml to induce GFP-CENP-E expression in DLD-1 cells. For siRNA treatment, Flp-In TRex-DLD-1 H2B-RFP cells were used as described (Kim et al., 2010). Cells were fixed and immunostained, and the images were collected at 0.2 μm z-sections with a 60×/1.42 PlanApo oil objective using a DeltaVision Core system (Applied Precision, Issaquah, WA) with CoolSNAP camera (Roper, Sarasota, FL). Images were deconvolved with SoftWoRx (Applied Precision), and maximum-intensity two-dimensional projections were assembled using FIJI (ImageJ; National Institutes of Health, Bethesda, MD).

Antibody and immunofluorescence

Cells were processed for immunofluorescence 48 h after siRNA treatment by fixing in 4% formaldehyde in MTSB (100 mM 1,4-piperazinediethanesulfonic acid [PIPES], pH 6.8, 0.1% Triton X-100, 0.1 mM $CaCl_2$, 1 mM $MgCl_2$), blocked overnight at 4°C in 2.5% fetal bovine serum, 0.2 M glycine, and 0.1% Triton X-100 in phosphate-buffered saline, followed by 1 h antibody incubation. CENP-E antibody HpX-1, anti-tubulin antibody DM1A (T9026; Sigma-Aldrich, St. Louis, MO), and anti–CENP-A antibody (13939; Abcam, Cambridge, MA) were used at 1:1000 and anti–centromere antibody ACA (15-234-0001; Antibodies Incorporated, Davis, CA) at 1:500. Cells were mounted in ProLong Gold (Invitrogen). Monopolar spindles were formed with 5 μM STLC for 2 h and 20 μM MG132 to prevent mitotic exit; GSK-923295 was used at 200 nM. To induce microtubule disassembly in cells with monopolar spindle, cells were treated for 20 min with a combination of 3.3 μM nocodazole and cold by incubating on a slurry of ice and water.

Microtubule signal was quantified by measuring the total pixel intensity of a 20-pixel-wide area along the spindle axis using FIJI, and local background was subtracted.

Live-cell imaging

DLD-1 cells expressing histone H2B–monomeric red fluorescent protein were seeded 24 h before experiment on Nunc LabTek II chambered coverglasses (Thermo Scientific, Waltham, MA). CO_2-independent medium (Life Technologies) was added, and the cells were imaged at 37°C for up to 2 h at 5 min intervals using a Delta-Vision Core system.

Protein purification

Tubulin was purified from cow brains by thermal cycling and chromatography, then labeled with rhodamine or Hilyte647. Kinesin 1 GFP construct K560 was purified as in Case et al. (1997). Xenopus laevis Truncated CENP-E labeled with GFP was expressed and purified from Escherichia coli as in Kim et al. (2008). X. laevis full-length CENP-E was expressed and purified from High Five cells (Invitrogen; (Abrieu et al., 2000). X. laevis Bonsai CENP-E was expressed in High Five cells. The cells were lysed using sonication in PK100 buffer (80 mM K PIPES, pH 6.8, 200 mM KCl, 20 mM imidazole, 0.5 mM ethylene glycol tetraacetic acid [EGTA], 1 mM $MgCl_2$, 0.1 mM MgATP, 1 mM dithiothreitol [DTT], protease inhibitors). The latter were prepared from one Complete EDTA-free protease inhibitor cocktail tablet (11 873 580 001; Roche, Basel, Switzerland) and phenylmethylsulfonyl fluoride, 0.2 mM. Cell lysate was spun 30 min at 15,000 rpm (Sorvall SA-600; Thermo Scientific). The supernatant was incubated for 1 h at 4°C with nickel-nitriloacetic acid beads and eluted using elution buffer (40 mM K-PIPES, pH 6.8, 80 mM KCl, 300 mM imidazole, 0.5 mM EGTA, 1 mM $MgCl_2$, 1 mM DTT, 0.1 mM MgATP). Peak fractions were collected, diluted 1:4 with HiTrap Q stabilizing buffer (20 mM K-PIPES, pH 6.8, 40 mM KCl, 1 mM $MgCl_2$, 0.5 mM EGTA, 1 mM DTT, 0.1 mM MgATP), and loaded into a HiTrap Q 1 ml column. Proteins were eluted using a 0.1–1 M KCl gradient in HiTrap Q elution buffer (25 mM K-PIPES, pH 6.8, 5 mM $MgCl_2$, 0.5 mM EGTA, 1 mM DTT, 0.1 mM ATP). Peak fractions were snap frozen after addition of 20% sucrose.

Work with CENP-E proteins in vitro

Microtubule gliding and single-molecule motility assays were carried out with a Nikon Eclipse Ti-E inverted microscope equipped with 100×/1.49 NA TIRF oil objective, Perfect Focus system, and TIRF Quad cube with emission wheels run with NIS-Elements Software. The temperature of the objective was kept at 32°C with a heater (Bioptechs, Butler, PA). The epifluorescence was excited with a 488 nm laser to visualize GFP and rhodamine and a 640 nm laser to visualize microtubules labeled with Hilyte647. Motility chambers were prepared with a glass slide, double-stick tape, and silanized 22 × 22 mm coverslips, as in Volkov et al. (2014). For experiments with soluble CENP-E, Taxol-stabilized, rhodamine-labeled

microtubules were attached to coverslips with anti-tubulin antibodies (Serotec), the surface was blocked with Pluronic-F127, and GFP-labeled proteins (0.5–3 nM) were imaged in the motility buffer composed of BRB80 (80 mM K-PIPES, 1 mM MgCl$_2$, 1 mM EGTA, pH 6.9) with 4 mg/ml bovine serum albumin (BSA), 2 mM DTT, 2 mM Mg-ATP, 7.5–10 µM Taxol, 6 mg/ml glucose, 68 µg/ml catalase, 0.1 mg/ml glucose oxidase, and 0.5% β-mercaptoethanol. Images were acquired with an Andor EMCCD at 100 ms/frame for each channel, and rhodamine and GFP signals were separated with emission filters. The number of GFP molecules in fluorescent dots for data in Supplemental Figure S1G was determined as in Gudimchuk *et al.* (2013). To visualize photobleaching steps, fluorescence curves were filtered with a Chung–Kennedy filter that preserves stepwise transitions (Chung and Kennedy, 1991), and the number of visual steps was counted (Supplemental Figure S1, H and I). Bonsai Ndc80-GFP protein, which is monomeric (Ciferri *et al.*, 2005), and processive kinesin 1 proteins were used as controls.

For microtubule-gliding assay, coverslips were coated with layers of biotin-BSA (22.5 µM), NeutrAvidin (25 µM), and biotinylated anti-GFP antibody (10–100 nM; Abcam) and then blocked with Pluronic F127 (1%) and another layer of biotin-BSA (22.5 µM) or biotin-PEG (100 µM; Quanta Biodesign, Plain City, OH). CENP-E proteins were added at 15–600 nM for 30 min to create coatings that were similar in density for different protein constructs, as judged by GFP brightness. After removal of the unbound protein, Taxol-stabilized, Hilyte647-labeled microtubules were imaged in the same motility buffer as before, except that β-mercaptoethanol was replaced with 10 mM DTT. Images were acquired once per second with 100- to 300 ms exposure and analyzed using ImageJ. Motility of CENP-E–coated beads was examined using instruments and procedures described in Gudimchuk *et al.* (2013). Fluorescence-based microtubule-pelleting assay was carried out as in Gudimchuk *et al.* (2013). Briefly, CENP-E proteins (6 nM) were incubated with increasing concentration of microtubules and 2 mM AMPPNP for 15 min at 32°C, microtubules were pelleted, and the concentration of unbound CENP-E was quantified by GFP fluorescence of the supernatants.

REFERENCES
Abrieu A, Kahana JA, Wood KW, Cleveland DW (2000). CENP-E as an essential component of the mitotic checkpoint in vitro. Cell 102, 817–826.

Blasius TL, Cai D, Jih GT, Toret CP, Verhey KJ (2007). Two binding partners cooperate to activate the molecular motor kinesin-1. J Cell Biol 176, 11–17.

Brown KD, Coulson RM, Yen TJ, Cleveland DW (1994). Cyclin-like accumulation and loss of the putative kinetochore motor CENP-E results from coupling continuous synthesis with specific degradation at the end of mitosis. J Cell Biol 125, 1303–1312.

Cai S, O'Connell CB, Khodjakov A, Walczak CE (2009). Chromosome congression in the absence of kinetochore fibres. Nat Cell Biol 11, 832–838.

Case RB, Pierce DW, Hom-Booher N, Hart CL, Vale RD (1997). The directional preference of kinesin motors is specified by an element outside of the motor catalytic domain. Cell 90, 959–966.

Chan GK, Schaar BT, Yen TJ (1998). Characterization of the kinetochore binding domain of CENP-E reveals interactions with the kinetochore proteins CENP-F and hBUBR1. J Cell Biol 143, 49–63.

Chung SH, Kennedy RA (1991). Forward-backward non-linear filtering technique for extracting small biological signals from noise. J Neurosci Methods 40, 71–86.

Ciferri C, De Luca J, Monzani S, Ferrari KJ, Ristic D, Wyman C, Stark H, Kilmartin J, Salmon ED, Musacchio A (2005). Architecture of the human ndc80-hec1 complex, a critical constituent of the outer kinetochore. J Biol Chem 280, 29088–29095.

Cleveland DW, Mao Y, Sullivan KF (2003). Centromeres and kinetochores: from epigenetics to mitotic checkpoint signaling. Cell 112, 407–421.

Coy DLD, Hancock WOW, Wagenbach MM, Howard JJ (1999). Kinesin's tail domain is an inhibitory regulator of the motor domain. Nat Cell Biol 1, 288–292.

Daum JR, Potapova TA, Sivakumar S, Daniel JJ, Flynn JN, Rankin S, Gorbsky GJ (2011). Cohesion fatigue induces chromatid separation in cells delayed at metaphase. Curr Biol 21, 1018–1024.

DeLuca JG, Gall WE, Ciferri C, Cimini D, Musacchio A, Salmon ED (2006). Kinetochore microtubule dynamics and attachment stability are regulated by Hec1. Cell 127, 969–982.

Ding X et al. (2010). Probing CENP-E function in chromosome dynamics using small molecule inhibitor syntelin. Cell Res 20, 1386–1389.

Espeut J, Gaussen A, Bieling P, Morin V, Prieto S, Fesquet D, Surrey T, Abrieu A (2008). Phosphorylation relieves autoinhibition of the kinetochore motor CENP-E. Mol Cell 29, 637–643.

Gudimchuk N, Vitre B, Kim Y, Kiyatkin A, Cleveland DW, Ataullakhanov FI, Grishchuk EL (2013). Kinetochore kinesin CENP-E is a processive bi-directional tracker of dynamic microtubule tips. Nat Cell Biol 15, 1079–1088.

Guo Y, Kim C, Ahmad S, Zhang J, Mao Y (2012). CENP-E-dependent BubR1 autophosphorylation enhances chromosome alignment and the mitotic checkpoint. J Cell Biol 198, 205–217.

Heuser J (1989). Protocol for 3-D visualization of molecules on mica via the quick-freeze, deep-etch technique. J Electron Microsc Tech 13, 244–263.

Huang TG, Hackney DD (1994). *Drosophila* kinesin minimal motor domain expressed in *Escherichia coli*. Purification and kinetic characterization. J Biol Chem 269, 16493–16501.

Huang TG, Suhan J, Hackney DD (1994). Drosophila kinesin motor domain extending to amino-acid position-392 is dimeric when expressed in *Escherichia coli*. J Biol Chem 269, 16502–16507.

Huang Y et al. (2012). CENP-E kinesin interacts with SKAP protein to orchestrate accurate chromosome segregation in mitosis. J Biol Chem 287, 1500–1509.

Jeppesen GM, Hoerber JKH (2012). The mechanical properties of kinesin-1: a holistic approach. Biochem Soc Trans 40, 438–443.

Kaan HYK, Hackney DD, Kozielski F (2011). The structure of the kinesin-1 motor-tail complex reveals the mechanism of autoinhibition. Science 333, 883–885.

Kapoor TM, Lampson MA, Hergert P, Cameron L, Cimini D, Salmon ED, McEwen BF, Khodjakov A (2006). Chromosomes can congress to the metaphase plate before biorientation. Science 311, 388–391.

Kim Y, Heuser JE, Waterman CM, Cleveland DW (2008). CENP-E combines a slow, processive motor and a flexible coiled coil to produce an essential motile kinetochore tether. J Cell Biol 181, 411–419.

Kim Y, Holland AJ, Lan W, Cleveland DW (2010). Aurora kinases and protein phosphatase 1 mediate chromosome congression through regulation of CENP-E. Cell 142, 444–455.

Liao HH, Li GG, Yen TJT (1994). Mitotic regulation of microtubule cross-linking activity of CENP-E kinetochore protein. Science 265, 394–398.

Maffini S et al. (2009). Motor-independent targeting of CLASPs to kinetochores by CENP-E promotes microtubule turnover and poleward flux. Curr Biol 1–15.

Maia ARRA, Garcia ZZ, Kabeche LL, Barisic MM, Maffini SS, Macedo-Ribeiro SS, Cheeseman IMI, Compton DAD, Kaverina II, Maiato HH (2012).

Cdk1 and Plk1 mediate a CLASP2 phospho-switch that stabilizes kineto-chore-microtubule attachments. J Cell Biol 199, 285–301.

Mao YY, Abrieu AA, Cleveland DWD (2003). Activating and silencing the mitotic checkpoint through CENP-E-dependent activation/inactivation of BubR1. Cell 114, 12–12.

McEwen BF, Chan GK, Zubrowski B, Savoian MS, Sauer MT, Yen TJ (2001). CENP-E is essential for reliable bioriented spindle attachment, but chromosome alignment can be achieved via redundant mechanisms in mammalian cells. Mol Biol Cell 12, 2776–2789.

Putkey FRF, Cramer TT, Morphew MKM, Silk ADA, Johnson RSR, McIntosh JRJ, Cleveland DWD (2002). Unstable kinetochore-microtubule capture and chromosomal instability following deletion of CENP-E. Dev Cell 3, 15–15.

Schaar BT, Chan GK, Maddox P, Salmon ED, Yen TJ (1997). CENP-E function at kinetochores is essential for chromosome alignment. J Cell Biol 139, 1373–1382.

Silk AD, Zasadil LM, Holland AJ, Vitre B, Cleveland DW, Weaver BA (2013). Chromosome missegregation rate predicts whether aneuploidy will promote or suppress tumors. Proc Natl Acad Sci USA 110, E4134–E4141.

Stevens JB et al. (2011). Diverse system stresses: common mechanisms of chromosome fragmentation. Cell Death Dis. 2, e178–e179.

Verhey KJ, Hammond JW (2009). Traffic control: regulation of kinesin motors. Nat Rev Mol Cell Biol 10, 765–777.

Volkov VA, Zaytsev AV, Grishchuk EL (2014). Preparation of segmented microtubules to study motions driven by the disassembling microtubule ends. J Vis Exp, doi:10.3791/51150.

Wan X et al. (2009). Protein architecture of the human kinetochore microtubule attachment site. Cell 137, 672–684.

Weaver BAA, Bonday ZQ, Putkey FR, Kops GJPL, Silk AD, Cleveland DW (2003). Centromere-associated protein-E is essential for the mammalian mitotic checkpoint to prevent aneuploidy due to single chromosome loss. J Cell Biol 162, 551–563.

Weaver BAA, Silk AD, Montagna C, Verdier-Pinard P, Cleveland DW (2007). Aneuploidy acts both oncogenically and as a tumor suppressor. Cancer Cell 11, 25–36.

Wong YL, Rice SE (2010). Kinesin's light chains inhibit the head-and microtubule-binding activity of its tail. Proc Natl Acad Sci USA 107, 11781–11786.

Wood KW et al. (2010). Antitumor activity of an allosteric inhibitor of centromere-associated protein-E. Proc Natl Acad Sci USA 107, 5839–5844.

Wood KWK, Sakowicz RR, Goldstein LSL, Cleveland DWD (1997). CENP-E is a plus end-directed kinetochore motor required for metaphase chromosome alignment. Cell 91, 10–10.

Yamada KH, Hanada T, Chishti AH (2007). The effector domain of human Dlg tumor suppressor acts as a switch that relieves autoinhibition of kinesin-3 motor GAKIN/KIF13B. Biochemistry 46, 10039–10045.

Yardimci H, van Duffelen M, Mao Y, Rosenfeld SS, Selvin PR (2008). The mitotic kinesin CENP-E is a processive transport motor. Proc Natl Acad Sci USA 105, 6016–6021.

Yen TJT, Compton DAD, Wise DD, Zinkowski RPR, Brinkley BRB, Earnshaw WCW, Cleveland DWD (1991). CENP-E, a novel human centromere-associated protein required for progression from metaphase to anaphase. EMBO J 10, 1245–1254.

Supplemental Materials
Molecular Biology of the Cell

Vitre et al.

Supplementary Figure Legends

Figure S1. In vitro assays and quantifications. (A) Prediction of coiled-coil regions in Bonsai CENP-E. The red double arrowhead corresponds to the amino acids sequence of the dimeric Truncated CENP-E. (B) Coomassie brilliant blue staining of a SDS PAGE of purified Bonsai CENP-E protein. (C) Schematic of the CENP-E conjugation to coverslips in microtubule gliding assay. (D) Schematic of bead motility assay, in which CENP-E coated beads are positioned on microtubule using laser trap, then the trap is turned off and beads velocity is measured. (E) Schematic representing TIRF assay with attached microtubules and soluble CENP-E molecules. (F) Representative two-color TIRF images of coverslip-attached microtubules with soluble GFP-labeled Bonsai CENP-E in 2mM ATP. Although small complexes of Bonsai CENP-E are readily observed as they adsorb non-specifically to the coverslip (yellow regions), on the microtubules (blue regions) clusters of Bonsai CENP-E molecules are seen. (G) Brightness of randomly selected fluorescent dots of Bonsai CENP-E bound to the coverslip (N=521, such as shown within yellow regions in panel F) and dots that co-localize with microtubules (N=115, such as shown within blue regions in panel F) based on 3 independent experiments. (H) Example photobleaching curves for GFP labeled proteins Ndc80, kinesin 1 and Bonsai CENP-E. (I) Fractions of the recordings with different number of steps, number of examined curves shown above each bar. (J) Initial brightness of dots formed by the indicated proteins before photobleaching.

Figure S2. Characterization of Bonsai CENP-E in vivo. (A) Schematic representing the Full length and the long, medium and short Bonsai Myc-Lap GFP tagged CENP-E proteins expressed in the DLD-1 cells following doxycycline treatment. (B) Immunoblot showing the levels of expression of the transgenes after 8 hours of doxycycline induction. (C) Immunofluorescence images of DLD-1 cells depleted of endogenous CENP-E and rescued with different CENP-E. The upper inset is a magnification of the metaphase plate area and the lower inset shows the spindle pole area. Cells stably express histone H2B-RFP. (D) Colony formation assays, cells were treated for two weeks in presence of doxycycline to induce expression of different transgenes. Endogenous protein was not depleted. The plot represents the mean colony number in two experiments. * $p < 0.05$; ** $p < 0.01$, p value of an unpaired t test realized on the mean of two independent experiments. Error bars represent SEM. (E) Representative images of DLD-1 cells rescued with Full length or Bonsai CENP-E; imaged from nuclear envelope breakdown (NEB) to anaphase onset. Time is in minutes. DNA is visualized using histone H2B-RFP reporter. The diagram represents the mean time from NEB to anaphase onset. Error bars represent SEM. At least two independent experiments are represented. *** $p < 0.001$, p value of an unpaired t test realized on the mean of, at least, two independents experiments.

Supplementary Video Legends

Video 1. Loss of chromosome alignment in a cell depleted of endogenous CENP-E and rescued with Full length CENP-E. Cells were arrested at metaphase and imaged live using H2B-RFP chromosomal marker. White arrowhead at 285 minutes indicates first visible loss of chromosome alignment.

Video 2. Loss of chromosome alignment in a cell depleted of endogenous CENP-E and rescued with Bonsai CENP-E. Cells were prepared and analyzed as in Video 1. White arrowhead at 138 minutes indicates first visible loss of chromosome alignment.
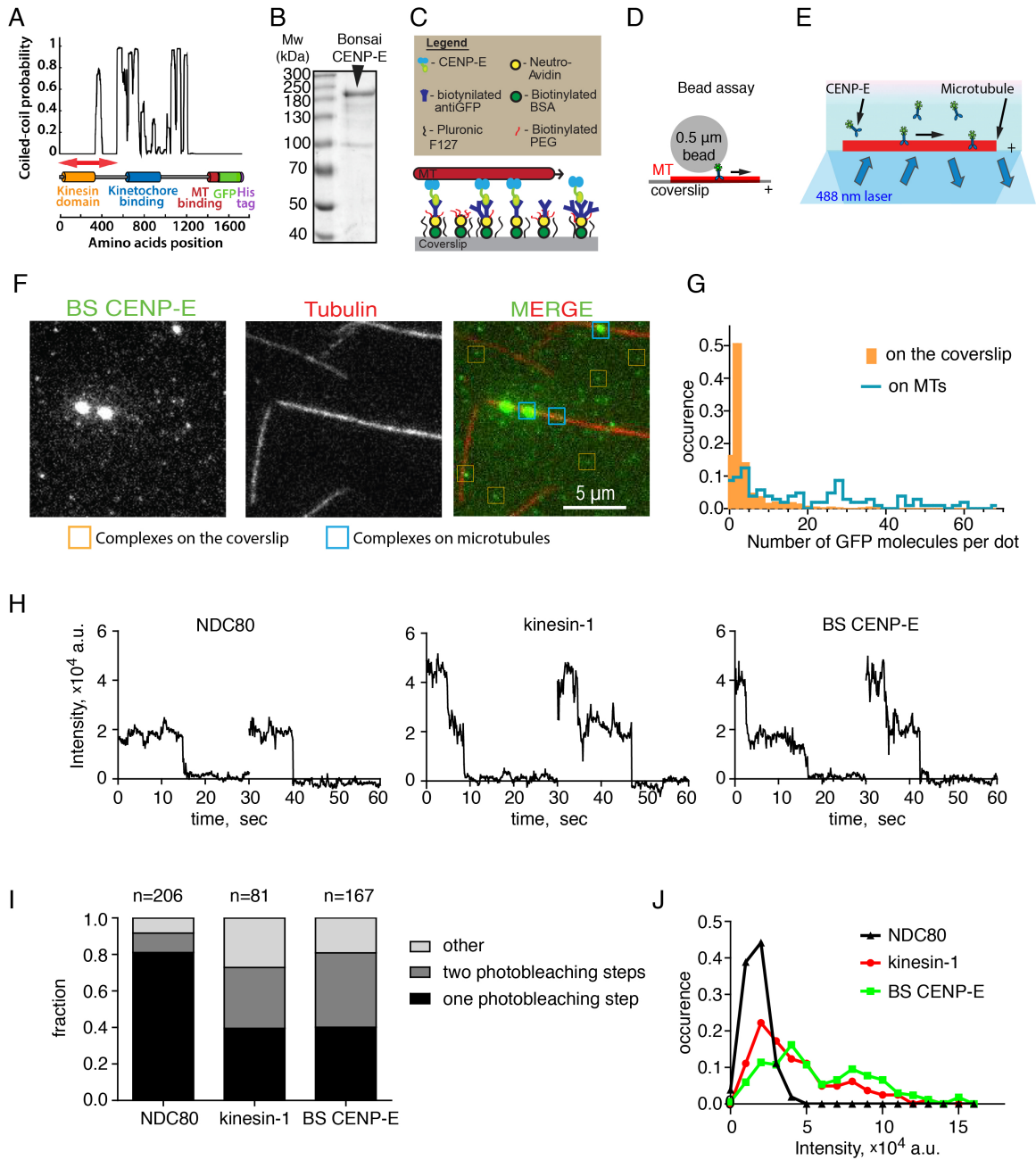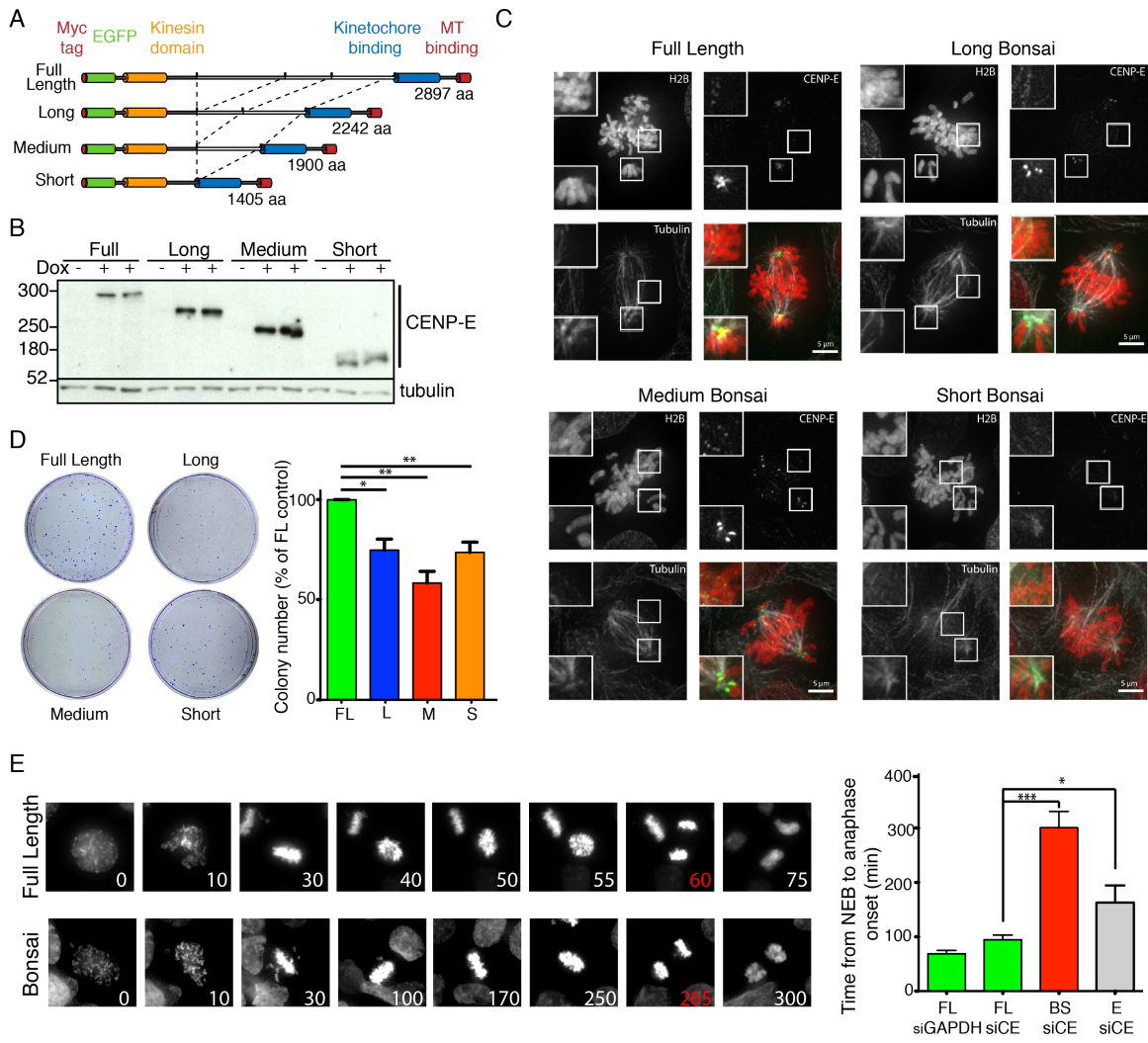
A

Coiled-coil probability

Kinesin domain | Kinetochore binding | MT binding | GFP | His tag

Amino acids position

B

Mw (kDa) — Bonsai CENP-E

300
250
180
130
100
70
50
40

C

Legend

- CENP-E
- Neutro-Avidin
- biotynilated antiGFP
- Biotinylated BSA
- Pluronic F127
- Biotinylated PEG

MT

Coverslip

D

Bead assay

0.5 μm bead

MT
coverslip +

E

CENP-E | Microtubule

488 nm laser

F

BS CENP-E | Tubulin | MERGE

5 μm

☐ Complexes on the coverslip ☐ Complexes on microtubules

G

occurence

on the coverslip
on MTs

Number of GFP molecules per dot

H

NDC80 | kinesin-1 | BS CENP-E

Intensity, ×10⁴ a.u.

time, sec | time, sec | time, sec

I

n=206 n=81 n=167

fraction

other
two photobleaching steps
one photobleaching step

NDC80 | kinesin-1 | BS CENP-E

J

occurence

NDC80
kinesin-1
BS CENP-E

Intensity, ×10⁴ a.u.

Figure S1

Figure S2